

RGB-Guided Resolution Enhancement of IR Images

Marcel Trammer^{1,2}, Nils Genser¹, and Jürgen Seiler²

¹ AI & Signal Processing Lab, Sielaff GmbH & Co. KG, Herrieden, Germany

² Multimedia Communications and Signal Processing,
Friedrich-Alexander-Universität Erlangen-Nürnberg (FAU), Erlangen, Germany

{m.trammer, n.genser} @sielaff.de, juergen.seiler @fau.de

Abstract—This paper introduces a novel method for RGB-Guided Resolution Enhancement of infrared (IR) images called Guided IR Resolution Enhancement (GIRRE). In the area of single image super resolution (SISR) there exists a wide variety of algorithms like interpolation methods or neural networks to improve the spatial resolution of images. In contrast to SISR, even more information can be gathered on the recorded scene when using multiple cameras. In our setup, we are dealing with multi image super resolution, especially with stereo super resolution. We consider a color camera and an IR camera. Current IR sensors have a very low resolution compared to color sensors so that recent color sensors take up 100 times more pixels than IR sensors. To this end, GIRRE increases the spatial resolution of the low-resolution IR image. After that, the upscaled image is filtered with the aid of the high-resolution color image. We show that our method achieves an average PSNR gain of 1.2 dB and at best up to 1.8 dB compared to state-of-the-art methods, which is visually noticeable.

Index Terms—multi-modal imaging, super resolution, image enhancement

I. INTRODUCTION

In distributed camera systems consisting of color cameras and infrared (IR) cameras, the spatial resolution typically differs by orders of magnitude. Latest IR sensors like Sony IMX 990 achieve a resolution of 1.3 MP [1]. In contrast, modern CMOS sensors like Sony IMX 411AQR reach a resolution of 151.4 MP [2]. This means, that modern color cameras can take up to 100 times as many pixels as IR cameras. Because of the higher number of pixels recorded, the color cameras record more spatial information about the scene than IR cameras. By using color information as additional source, we propose to increase the spatial resolution of IR cameras. Therefore, our novel Guided IR Resolution Enhancement (GIRRE) algorithm first increases the spatial resolution of the low-resolution IR image. Then, this newly generated image is filtered with the help of the high-resolution color image to restore missing high-frequent information in the IR image. Up to now, we assume our setup consisting of one color camera and one IR camera. Furthermore, we assume that the images are already well registered, for example by methods as proposed in [3], [4].

In order to understand what possibilities we have to increase the spatial resolution, we will give an overview of the state of the art in Section II. In Section III, we introduce our novel method. To demonstrate the improvement against the state-of-the-art methods, we evaluate our method with respect to different databases, multiple scale factors, and latest state-of-the-art algorithms in Section IV.

II. STATE OF THE ART

Today’s smartphones are usually equipped with several cameras [5], [6]. When using multiple cameras, it is obvious to equip them with different modalities to achieve more information of the recorded scene. For example, a combination of a color camera and an IR camera is often used. One of the most common examples is the Apple iPhone True Depth IR system. This allows depth measurements to be taken and the state of human health to be determined [7].

In the field of distributed multi-modal camera systems, a huge challenge can be the different spatial resolution of the various cameras. In contrast to recently published methods like the Camera Array for Multi-Spectral Imaging [3], which contains identical cameras, we combine an IR camera with a color camera in our setup. The combination of IR camera and color camera leads to the problem of different spatial resolutions that may differ by orders of magnitude. In practice, the IR cameras have lower spatial resolution as an identically constructed color camera. A huge task in such a setup is to increase the spatial resolution of an IR image to the spatial resolution of a color image. In order to increase spatial resolution there are different approaches, which will be discussed next.

On the one hand, the field of single image super resolution (SISR) is well known. SISR reconstructs a high-resolution image from a low-resolution image [8]. Solving the problem of SISR in research is very common and there are two different concepts. First, different interpolation methods such as bicubic interpolation can be mentioned among many others. Bicubic interpolation is a common method in the field of SISR which is well studied and introduces only minor computational complexity [9]. Moreover, deep neuronal networks can be mentioned. Accurate Image Super-Resolution using Very Deep Convolutional Networks (VDSR) was one important milestone in the field of SISR. One important aspect is, that VDSR uses an interpolated image as input. The main idea to train VDSR is to learn the residual between the output image and the input image [10], [11]. Furthermore, Enhanced Deep Residual Networks for single Image Super-Resolution (EDSR) should be mentioned. In contrast to VDSR, EDSR does not use an interpolated image, instead the network uses the low-resolution image directly. In order to use the image directly, EDSR was trained separately for each scaling [12], [13].

On the other hand, the field of multi image super resolution (MISR) can be named. To achieve a higher spatial resolution of an image, MISR combines multiple images from the same scene [14]. To capture multiple images from one scene, there

are various options. One is video super resolution (VSR). In VSR, the datasets are ordered frames of the same scene. To achieve a high-resolution image at time $t = T$, temporally adjacent images can be used [15]. Another approach is stereo super resolution (SSR). SSR captures two images from different positions simultaneously from the same scene. Among other things, this leads to the parallax effect. This effect has to be compensated by algorithms [16], [17].

Since capturing infrared images requires larger exposure times, one can receive huge movements between consecutive images. This increases the difficulty to find corresponding image regions between consecutive images [15]. Capturing a moving scene with large exposure times results in motion blur [18]. Because of that, VSR is not an option in our considered scenario. That is why we go into the field of SSR. Unlike [19] and [20], we have a high-resolution color image and a low-resolution IR image.

III. GUIDED IR RESOLUTION ENHANCEMENT (GIRRE)

In the following, we introduce our Guided IR Resolution Enhancement (GIRRE) method. The algorithm increases the spatial resolution of the low-resolution IR image \tilde{X} to the same spatial resolution as that of the high-resolution color image G . We obtain the approximated image \tilde{X} . Similar to [21], we assume that the enhanced image \hat{X} is a local linear transformation of the high-resolution color image G . Moreover, GIRRE uses the guided filter that was introduced in [21] to transfer the information contained in the high-resolution color image G to the approximated image \tilde{X} . In the following, we describe the proposed GIRRE algorithm.

Because the method is independent of the color depth, we assume the image values to be between zero and one and are of floating point accuracy. As shown in Fig. 1, a function u upscales the low-resolution IR image \tilde{X} to the size of the high-resolution color image G to obtain the approximated image \tilde{X} :

$$u(\tilde{X}) = \tilde{X}. \quad (1)$$

Afterwards, we use a transfer function $t_{r,\epsilon}$ to increase the image quality of the approximated image \tilde{X} with the help of the high-resolution color image G to receive the enhanced image \hat{X} :

$$t_{r,\epsilon}(\tilde{X}, G) = \hat{X}. \quad (2)$$

The transfer function $t_{r,\epsilon}$ accepts two parameters. The radius r , which describes a square window ω_k centered around the considered pixel k and ϵ as regularization parameter. Next, we assume the enhanced image \hat{X} is a local linear transformation of the guide image G :

$$\hat{X}_i = a_k G_i + b_k, \forall i \in \omega_k, \quad (3)$$

where (a_k, b_k) are linear coefficients which are constant in the window ω_k and i being the pixels in the window. The local linear model ensures that \hat{X} has an edge if G has an edge, because $\nabla \hat{X} = a \nabla G$. To calculate the coefficients, we need the following assumption. The enhanced image \hat{X}_i is equal to the approximated image \tilde{X}_i subtracting some distortions η_i like noise:

$$\hat{X}_i = \tilde{X}_i - \eta_i. \quad (4)$$

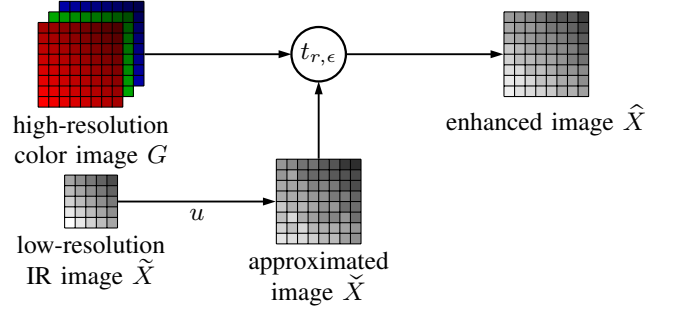


Fig. 1: First, the proposed method GIRRE increases the spatial resolution of \tilde{X} . After that, the function $t_{r,\epsilon}$ uses the color image G to generate details in the approximated IR image \tilde{X} .

To achieve minimal distortions, we minimize the difference between \hat{X} and \tilde{X} while keeping the linear model (3). Especially, in the window ω_k , we minimize the cost function:

$$E(a_k, b_k) = \sum_{i \in \omega_k} \left((a_k G_i + b_k - \tilde{X}_i)^2 + \epsilon a_k^2 \right). \quad (5)$$

The parameter ϵ controls the influence of large a_k . Equation (5) is the *linear ridge regression* model [22], [23] with the solution:

$$a_k = \frac{\frac{1}{|\omega_k|} \sum_{i \in \omega_k} G_i \tilde{X}_i - \mu_k \bar{X}_k}{\sigma_k^2 + \epsilon}, \quad (6)$$

$$b_k = \bar{X}_k - a_k \mu_k, \quad (7)$$

with $|\omega_k|$ being the cardinality of ω_k and μ_k, σ_k^2 the mean and variance of G in ω_k and \bar{X}_k the mean of \tilde{X} in ω_k . After calculating the parameters a_k and b_k , we are able to compute the output \hat{X}_i with respect to (3).

The problem is, that a pixel k is involved in all overlapping windows ω_i which contain k . Here, ω_i denote a window at a random pixel i . Thus, we receive different values for \bar{X}_k in (3) for different windows. Consequently, the strategy is to average all the values of \hat{X}_k :

$$\hat{X}_k = \frac{1}{|\omega_i|} \sum_{i|k \in \omega_i} (a_i G_k + b_i). \quad (8)$$

Because of the symmetrical window ω_i , the following applies:

$$\sum_{i|k \in \omega_i} a_i = \sum_{i \in \omega_k} a_i. \quad (9)$$

With (9), we can write (8) as:

$$\hat{X}_k = \bar{a}_k G_k + \bar{b}_k, \quad (10)$$

with $\bar{a}_k = \frac{1}{|\omega_k|} \sum_{i \in \omega_k} a_i$ and $\bar{b}_k = \frac{1}{|\omega_k|} \sum_{i \in \omega_k} b_i$ being the average coefficients of all windows which overlap the pixel k . A pseudocode for GIRRE is shown in Algorithm 1.

To sum up, GIRRE scales up the spatial resolution of a low-resolution infrared image with the help of a high-resolution color image. Therefore, we assume a local linear dependency of the images in order to be able to apply the presented algorithm.

Algorithm 1 Proposed GIRRE algorithm

Input \tilde{X} low-resolution infrared image
 G high-resolution color image**Output** \hat{X} enhanced image

- 1: upscale \tilde{X} to the size of G in (1)
 - 2: **for all** $i \in |\tilde{X}|$ **do** $\triangleright (|\tilde{X}|: \text{cardinality of } \tilde{X})$
 - 3: compute a_i in (6)
 - 4: compute b_i in (7)
 - 5: **end for**
 - 6: **for** $k \in |\tilde{X}|$ **do**
 - 7: compute the average of the a_i , such that $i \in \omega_k$
 - 8: compute the average of the b_i , such that $i \in \omega_k$
 - 9: compute \tilde{X}_k in (10)
 - 10: **end for**
-

IV. EVALUATION

Before evaluating the proposed GIRRE method, we will discuss the employed parameters. In literature, it is common to use scaling factors of 2×2 , 3×3 and 4×4 [24], [25]. Moreover we use a scaling of 8×8 , because color images contain up to 100 times more pixels than infrared images so that our calculations become even more practical. A scaling $x \times y$ means, that we scale the width by a factor of x and the height by a factor of y .

For evaluation, we selected the databases CAVE [26], Harvard [27] and TokyoTech [28]. The datasets are chosen, because the different spectra are captured with a tunable filter. For this reason, we can assume the images to be well registered. The CAVE dataset contains grayscale images between 400 nm and 700 nm and a color image which is rendered by the grayscale images at different wavelengths. Furthermore, the Harvard dataset contains grayscale images between 420 nm and 720 nm but without color images. TokyoTech contains images in the range of 420 nm to 650 nm (visible) and for 650 nm to 1000 nm (IR). Like Harvard, TokyoTech does not include a color image. For the TokyoTech and Harvard datasets, we use [29] to generate color images. The image size of the CAVE and TokyoTech datasets are 512×512 pixels. The images of the Harvard dataset are resized to the same spatial resolution. Furthermore, for visual examples we use a spatial resolution of 512×512 pixels, too. To simulate the low-resolution IR image \tilde{X} , we downscale the respective IR ground truth image by the considered scale factor. For the analysis, we select the image with the longest wavelength from each of the data sets as the ground truth image.

As shown in Section III, radius r and the regularization parameter ϵ are essential for the transfer function $t_{r,\epsilon}$. Irrespective of the scale factor, the evaluation with the TokyoTech database has shown that we obtain the best results for $\epsilon = 0.1^4$. The radius r behaves differently from ϵ since it depends on the scale factor and the upscale function u . In order to find the radius, we therefore choose TokyoTech as reference dataset for all functions u . The chosen radius has the biggest difference in terms of peak signal-to-noise ratio (PSNR) between the approximated image and GIRRE. The determined parameters are shown in Table I.

The following evaluations are carried out on the Harvard

TABLE I: Parameters for the transfer function $t_{r,\epsilon}$ of the proposed GIRRE method optimized on TokyoTech. Parameter ϵ has a fixed value of 0.1^4 . The value for the radius depends on the scaling and the procedure how the approximated image \tilde{X} is computed. The table shows the radius per scaling for $\tilde{X}_{\text{BICUBIC}}$ and \tilde{X}_{VDSR} .

scale	radius	scale	radius
2×2	1	2×2	2
3×3	3	3×3	3
4×4	6	4×4	4
8×8	15	8×8	15

(a) $\tilde{X}_{\text{BICUBIC}}$ (b) \tilde{X}_{VDSR}

TABLE II: Comparison of the proposed GIRRE algorithm with respect to BICUBIC[9] on multiple datasets in terms of PSNR.

Scale	Radius	Dataset	GIRRE	BICUBIC[9]	DIFF
2×2	1	Harvard[27]	34.22	33.63	0.59
		CAVE[26]	41.19	40.62	0.57
		Average	37.71	37.12	0.59
3×3	3	Harvard[27]	32.47	31.25	1.22
		CAVE[26]	38.12	36.74	1.38
		Average	35.30	34.00	1.30
4×4	6	Harvard[27]	31.45	29.93	1.52
		CAVE[26]	36.44	34.56	1.88
		Average	33.95	32.25	1.70
8×8	15	Harvard[27]	29.08	27.38	1.70
		CAVE[26]	32.14	29.86	2.28
		Average	30.61	28.62	1.99

and CAVE datasets, which are independent of the TokyoTech dataset that has been used for parameter optimization. Table II shows the PSNR in decibel (dB) for our proposed GIRRE method with bicubic interpolation as upscale function u and for bicubic interpolation as competing method. The last column shows the difference between GIRRE and bicubic interpolation. If the difference is positive, our method increases in terms of the PSNR. When it is negative, our method decreases the PSNR. For the table, we have a multi index. This means, that we group the table by scale factor, radius and dataset. The radius has a one-to-one relationship with the scale factor. As last level, we have different datasets and an extra row for the average value in each group. We highlight the best method in bold letters. Furthermore, the radius increases by enlarging the scaling. This can be explained by the fact that the function $t_{r,\epsilon}$ requires more information to enhance the image. From Table II, we can infer that the proposed method significantly increases PSNR for all datasets by scaling 2×2 up to 8×8 . The gain in terms of the PSNR is between 0.57 dB and 2.28 dB. For bicubic interpolation as upscale function u , we increase the PSNR on average by 1.39 dB.

In the following, we compare our novel GIRRE method to VDSR[10], which is a recent super-resolution method based on a neuronal network. Table III has the same structure as Table II. Here, the approximated image \tilde{X} was generated with the upscale function $u = \text{VDSR}[10]$. In this case, we increase PSNR by at least 1.75 dB. For scaling 2×2 and the Harvard dataset, we achieve the best result with a difference of 2.79 dB. On average over all datasets, we increase PSNR by 2.37 dB with GIRRE

TABLE III: Comparison of the proposed GIRRE algorithm with respect to VDSR[10] on multiple datasets in terms of PSNR.

Scale	Radius	Dataset	GIRRE	VDSR[10]	DIFF
2×2	2	Harvard[27]	36.23	33.44	2.79
		CAVE[26]	41.83	39.55	2.28
		Average	39.03	36.49	2.54
3×3	3	Harvard[27]	33.86	31.13	2.73
		CAVE[26]	39.24	36.63	2.61
		Average	36.55	33.88	2.67
4×4	4	Harvard[27]	32.34	30.33	2.01
		CAVE[26]	37.60	35.23	2.37
		Average	34.97	32.78	2.19
8×8	15	Harvard[27]	29.11	27.36	1.75
		CAVE[26]	32.18	29.77	2.41
		Average	30.64	28.57	2.07

TABLE IV: Comparison of the proposed GIRRE method with bicubic interpolation[9] and EDSR[12]. The table shows the PSNR (SSIM) scores.

Scale	GIRRE	BICUBIC[9]	EDSR[12]
2×2	39.03 (0.95)	37.12 (0.93)	38.47 (0.94)
3×3	36.55 (0.92)	34.00 (0.88)	35.18 (0.89)
4×4	34.97 (0.90)	32.25 (0.84)	33.20 (0.85)
8×8	30.64 (0.86)	28.62 (0.76)	29.65 (0.78)

compared to VDSR[10].

Tables II and III show, that on all considered scalings the proposed GIRRE method with upscale function $u = \text{VDSR}$ achieves a higher PSNR in contrast to GIRRE with upscale function $u = \text{BICUBIC}$. That is why we choose $u = \text{VDSR}$ for further evaluations.

Table IV shows the PSNR in dB and the structural similarity index measure (SSIM) in brackets of GIRRE and the state-of-the-art method BICUBIC[9]. Furthermore, since BICUBIC[9] is a simple and old method, we also compare GIRRE with EDSR[12]. The difference in PSNR increases from scaling 2×2 to 4×4 and then decreases. Furthermore, the difference of the SSIM increases from the smallest considered scaling to the largest considered scaling. This behavior is observed for both state-of-the-art methods. Furthermore, GIRRE has the best PSNR and SSIM over the state-of-the-art methods for scaling 2×2 to 8×8 which we mark as bold.

To conclude the evaluation, we give some visual examples. Fig. 2 shows a section of the *chart_and_stuffed_toy* image of the CAVE dataset. The first row shows the ground truth image, the low-resolution IR image and the enhanced image GIRRE. The high-resolution color image, the enhanced image BICUBIC[9] and the enhanced image EDSR[12] are shown at the second row. Furthermore, we added the PSNR scores to the images and mark the highest PSNR value in bold letters. To achieve the processed images, we use a 4×4 scaling. This results in a spatial resolution of 128×128 of the low-resolution IR image. The image section shows the hair of a stuffed toy as well as a chart. For this example, our method achieves 33.55 dB. The best state-of-the-art method EDSR[12] achieves only 31.00 dB, which leads to a difference of 2.55 dB. This can be noticed for all state-of-the-art methods. For example, the numbers 3, 4, and 5 can only be recognized on the image reconstructed by GIRRE.

Finally, Fig. 3 shows *img1* of the Harvard dataset. The

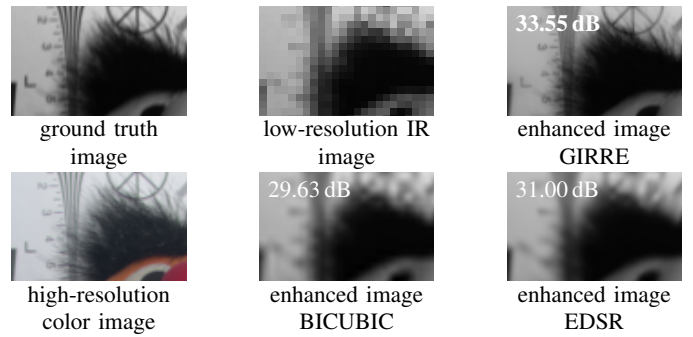


Fig. 2: Image detail of *chart_and_stuffed_toy* from CAVE with PSNR value between ground truth and the image by scaling 4×4 .

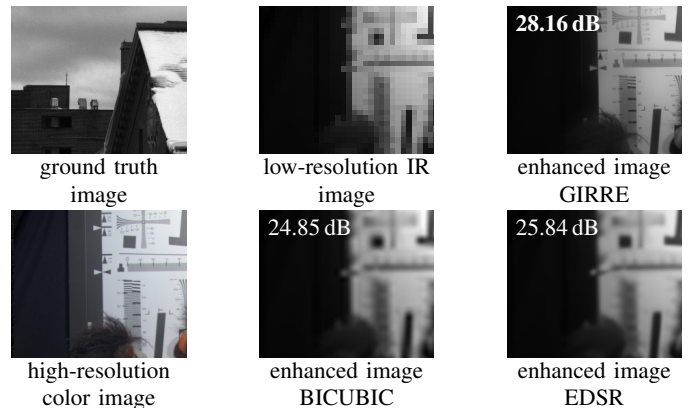


Fig. 3: Image detail of *img1* from Harvard with PSNR value between ground truth and the image by scaling 8×8 .

structure is like in Fig. 2, but using an 8×8 scaling. The low-resolution IR image has a resolution of 64×64 . In the middle of the image, we can see a ventilation inlet. Our method shows sharp edges for the ventilation inlet. In this example, we can increase PSNR by 2.32 dB with respect to the best state-of-the-art method EDSR[12].

V. CONCLUSION

Modern electronic devices such as smartphones use multi-modal stereo cameras. Especially, the combination of a color camera and an IR camera is widely employed. However, a major problem is the huge difference between the spatial resolution of current sensors. Recent color sensors typically take 100 times more pixels than current infrared sensors. For this reason, color images contain significantly more spatial information of the scene than infrared images.

To this end, we introduce the novel Guided IR Resolution Enhancement (GIRRE) algorithm to increase the quality of low-resolution infrared images with the help of high-resolution color images. In Table IV, we showed that our method achieves an average gain of 1.2 dB and at best we can increase the PSNR by 1.8 dB compared to EDSR[12]. Furthermore, we demonstrated the superiority of our method by giving visual examples.

In sum, the quality of low-resolution infrared images can be significantly improved with the aid of high-resolution color images when using the proposed GIRRE algorithm.

REFERENCES

- [1] SWIR Image Sensor. Accessed: 23.03.2023. [Online]. Available: <https://www.sony-semicon.com/en/products/is/industry/swir.html>
- [2] Rolling Shutter Image Sensor. [Online]. Available: <https://www.sony-semicon.com/en/products/is/industry/rolling-shutter.html>
- [3] N. Genser, J. Seiler, and A. Kaup, "Camera array for multi-spectral imaging," *IEEE Transactions on Image Processing*, vol. 29, pp. 9234–9249, 2020.
- [4] T. Zhi, B. R. Pires, M. Hebert, and S. G. Narasimhan, "Deep material-aware cross-spectral stereo matching," in *Proc. IEEE/CVF Conference on Computer Vision and Pattern Recognition (CVPR)*, 2018, pp. 1916–1925.
- [5] Y. Hwang, K. Byon, and J. Kim, "Camera module including multi-lens and electronic device having the same," Patent WO/2017/048 081, Mar. 2017.
- [6] W. K. Park, J. W. Kim, J. Y. Park, S. J. Hwang, I. C. Shim, D. H. Jeong, B. G. An, D. W. Kim, and K. H. Choi, "Dual camera module and portable electronic device," U.S. Patent 11,048,307, Jun. 2021.
- [7] N. Genser, A. Spruck, J. Seiler, and A. Kaup, "Deep learning based cross-spectral disparity estimation for stereo imaging," in *Proc. IEEE International Conference on Image Processing (ICIP)*, 2020, pp. 2536–2540.
- [8] M. Irani and S. Peleg, "Improving resolution by image registration," *CVGIP: Graphical Models and Image Processing*, vol. 53, no. 3, pp. 231–239, 1991.
- [9] I. Amidror, "Scattered data interpolation methods for electronic imaging systems: a survey," *Journal of Electronic Imaging*, vol. 11, no. 2, pp. 157 – 176, 2002.
- [10] J. Kim, J. K. Lee, and K. M. Lee, "Accurate image super-resolution using very deep convolutional networks," in *Proc. IEEE Conference on Computer Vision and Pattern Recognition (CVPR)*, 2016, pp. 1646–1654.
- [11] G. Yang, Z. Chen, D. L. Ndzi, L. Yang, A.-H. Al-Hassani, D. C. Paul, Z. Duan, and J. Chen, "Deep spatial interpolation of rain field for u.k. satellite networks," *IEEE Transactions on Antennas and Propagation*, vol. 71, no. 2, pp. 1793–1803, 2023.
- [12] B. Lim, S. Son, H. Kim, S. Nah, and K. M. Lee, "Enhanced deep residual networks for single image super-resolution," in *Proc. IEEE Conference on Computer Vision and Pattern Recognition Workshops (CVPRW)*, 2017, pp. 1132–1140.
- [13] K. Chauhan, S. N. Patel, M. Kumhar, J. Bhatia, S. Tanwar, I. E. Davidson, T. F. Mazibuko, and R. Sharma, "Deep learning-based single-image super-resolution: A comprehensive review," *IEEE Access*, vol. 11, pp. 21 811–21 830, 2023.
- [14] T. Richter and A. Kaup, "Super-resolution for differently exposed mixed-resolution multi-view images adapted by a histogram matching method," in *Proc. IEEE International Conference on Acoustics, Speech and Signal Processing (ICASSP)*, 2017, pp. 2022–2026.
- [15] X. Tao, H. Gao, R. Liao, J. Wang, and J. Jia, "Detail-revealing deep video super-resolution," in *Proc. IEEE International Conference on Computer Vision (ICCV)*, 2017, pp. 4482–4490.
- [16] L. Wang, Y. Wang, Z. Liang, Z. Lin, J. Yang, W. An, and Y. Guo, "Learning parallax attention for stereo image super-resolution," in *Proc. IEEE/CVF Conference on Computer Vision and Pattern Recognition (CVPR)*, 2019, pp. 12 242–12 251.
- [17] Z. Wang, J. Chen, and S. C. H. Hoi, "Deep learning for image super-resolution: A survey," *IEEE Transactions on Pattern Analysis and Machine Intelligence*, vol. 43, no. 10, pp. 3365–3387, 2021.
- [18] Z. Ma, R. Liao, X. Tao, L. Xu, J. Jia, and E. Wu, "Handling motion blur in multi-frame super-resolution," in *2015 IEEE Conference on Computer Vision and Pattern Recognition (CVPR)*, 2015, pp. 5224–5232.
- [19] M. Bätz, A. Eichenseer, J. Seiler, M. Jonscher, and A. Kaup, "Hybrid super-resolution combining example-based single-image and interpolation-based multi-image reconstruction approaches," in *Proc. IEEE International Conference on Image Processing (ICIP)*, 2015, pp. 58–62.
- [20] L. T. Sach, K. Atsuta, K. Hamamoto, and S. Kondo, "A robust stereo matching method for low texture stereo images," in *Proc. IEEE-RIVF International Conference on Computing and Communication Technologies (ICCCCT)*, 2009, pp. 1–8.
- [21] K. He, J. Sun, and X. Tang, "Guided image filtering," *IEEE Transactions on Pattern Analysis and Machine Intelligence*, vol. 35, no. 6, pp. 1397–1409, 2013.
- [22] T. Hastie, R. Tibshirani, and J. Friedman, *The Elements of Statistical Learning*. Springer New York, NY, 2009.
- [23] N. Draper and H. Smith, *Applied Regression Analysis, Third Edition*. John Wiley & Sons, Ltd, 2014.
- [24] T. Richter, J. Seiler, W. Schnurrer, M. Bätz, and A. Kaup, "Combining single-image and multiview super-resolution for mixed-resolution image plus depth data," in *Proc. 23rd European Signal Processing Conference (EUSIPCO)*, 2015, pp. 1840–1844.
- [25] M. Shoeiby, A. Robles-Kelly, R. Timofte, R. Zhou, F. Lahoud, S. Süsstrunk, Z. Xiong, Z. Shi, C. Chen, D. Liu, Z.-J. Zha, F. Wu, K. Wei, T. Zhang, L. Wang, Y. Fu, K. Nagasubramanian, A. K. Singh, A. Singh, S. Sarkar, and B. Ganapathysubramanian, "Pirm2018 challenge on spectral image super-resolution: Methods and results," in *Proc. Computer Vision – ECCV 2018 Workshops*, L. Leal-Taixé and S. Roth, Eds. Cham: Springer International Publishing, 2019, pp. 356–371.
- [26] F. Yasuma, T. Mitsunaga, D. Iso, and S. K. Nayar, "Generalized Assorted Pixel Camera: Postcapture Control of Resolution, Dynamic Range, and Spectrum," *IEEE Transactions on Image Processing*, vol. 19, no. 9, pp. 2241–2253, 2010.
- [27] A. Chakrabarti and T. Zickler, "Statistics of Real-World Hyperspectral Images," in *Proc. IEEE Conference on Computer Vision and Pattern Recognition (CVPR)*, 2011, pp. 193–200.
- [28] Y. Monno, H. Teranaka, K. Yoshizaki, M. Tanaka, and M. Okutomi, "Single-sensor rgb-nir imaging: High-quality system design and prototype implementation," *IEEE Sensors Journal*, vol. 19, no. 2, pp. 497–507, 2019.
- [29] M. Magnusson, J. Sigurdsson, S. E. Armansson, M. O. Ulfarsson, H. Deborah, and J. R. Sveinsson, "Creating RGB images from hyperspectral images using a color matching function," in *Proc. IEEE International Geoscience and Remote Sensing Symposium (IGARSS)*, 2020, pp. 2045–2048.